Available online at www.sciencedirect.com
SCIENCE DIRECT®
Journal of Computational Physics 214 (2006) 171–186
JOURNAL OF COMPUTATIONAL PHYSICS
www.elsevier.com/locate/jcp

Efficient electric resistivity inversion using adjoint state of mixed finite-element method for Poisson's equation

Taeyoung Ha [a,*], Sukjoon Pyun [b], Changsoo Shin [c]

[a] *Department of Mathematical Sciences, Seoul National University, San 56-1, Sillim-dong, Gwanak-gu, Seoul 151-747, Republic of Korea*
[b] *Computational Science and Technology Program, Seoul National University, San 56-1, Sillim-dong, Gwanak-gu, Seoul 151-742, Republic of Korea*
[c] *School of Civil, Urban and Geosystem Engineering, Seoul National University, San 56-1, Sillim-dong, Gwanak-gu, Seoul 151-742, Republic of Korea*

Received 11 February 2005; received in revised form 23 August 2005; accepted 14 September 2005
Available online 25 October 2005

Abstract

We propose an electric resistivity inversion method that is similar to the reverse time migration technique applied to seismic data. For calculating model responses and inversion, we use the mixed finite-element method with the standard $P_1 - P_0$ pair for triangular decompositions, which makes it possible to compute both the electric potential and the electric field vector economically. In order to apply the adjoint state of the Poisson equation in the resistivity inverse problem, we introduce an apparent electric field defined as the dot product between the computed electric field vector and a weighting factor and then defining a virtual source to compute the partial derivative of the electric field vector. We exploit the adjoint state (the symmetry of Green's function) of matrix equations derived from solving the Poisson equation by the mixed finite-element method, for the calculation of the steepest descent direction of our objective function. By computing the steepest descent direction by a dot product of backpropagated residual and virtual source, we can avoid the cumbersome and expensive process of computing the Jacobian matrix directly. We calibrate our algorithm on a synthetic of a buried conductive block and obtain an image that is compatible with the limits of the resistivity method.

Keywords: Resistivity inversion; Mixed finite-element method; Steepest descent method

1. Introduction

Electric resistivity inversion has been used as an interpretation tool for generating subsurface structures from voltage differences measured on the surface in a dc survey. Geophysicists and applied mathematicians have studied electric resistivity inversion techniques using integral equation [1], alpha center [22], Born approximation [13], finite-difference [6,37], finite-element [5,9,26], boundary-element methods [14,17,35] and multiscale methods [21]. In particular, Pain et al. [20] proposed the inverse algorithm for 3D anisotropic media.

* Corresponding author. Tel.: +82 2 880 6271; fax: +82 2 887 4694.
E-mail addresses: tyha@math.snu.ac.kr (T. Ha), pyunsj@gpl.snu.ac.kr (S. Pyun), css@model.snu.ac.kr (C. Shin).

0021-9991/$ - see front matter
doi:10.1016/j.jcp.2005.09.007

A majority of these methods are equally valuable for solving other geophysical problems such as the inversion of electromagnetic and seismic data by constructing appropriate objective functions. Although global optimization schemes such as simulated annealing and genetic algorithms are frequently used in geophysical problems, geophysicists still favor local optimization methods since local optimization methods are computationally efficient compared with global search methods. Many applied mathematicians can also apply these methods in the medical fields with electric impedance tomography [2,4,7,8].

This study focuses on resistivity inversion using local optimization, especially the steepest descent method. In general, the local minimization problems such as Gauss–Newton method and steepest descent method are the most widely used for its fast convergence, and the steepest descent direction is calculated most efficiently with the Jacobian computed from the reciprocity theorem of Green function in conductivity problem [26,31,32,36]. The reciprocity approach is a very efficient method for constructing the Jacobian or gradient and Shin et al. [28] also applied this method to seismic waveform inversion. At the same time, Gauss–Newton method has a disadvantage in that it requires a large core memory to save all of the Green functions corresponding to every source and receiver position and incurs the large overhead computing cost to calculate the Jacobian matrix [28].

Lailly [12], Tarantola [29] and Pratt et al. [23] developed a novel way of determining the steepest descent direction for seismic inversion in reverse time migration. Pratt et al. [23] predicted that the seismic waveform inversion algorithm could be easily applied to dc and electromagnetic problems. In this study, we propose an electric resistivity inversion algorithm that is similar to a recent seismic inversion algorithm [28,23] that employs the adjoint state of the wave equation. The backpropagation algorithm of seismic inversion and reverse time migration, in general, uses the adjoint state of the forward modeling operator of the wave equation. However, in a dc resistivity problem solving Poisson's equation by standard finite-element or finite-difference method, we have found a resulting capacity matrix which cannot be directly used to backpropagate residual electric field vector as we backpropagate the residual in the seismic waveform inverse problem. To circumvent this problem, we must define an equivalent apparent electric field measurement, and compute both electric potential and electric field vector using a mixed finite-element method. In this way, we can build a new objective function as an l_2-norm of residuals between measured apparent resistivity and modeled apparent resistivity, thereby allowing us to employ the adjoint state of mixed finite-element method for the implicit computation of the steepest descent direction without computing the Jacobian matrix.

In the following sections, we will introduce a governing equation used for electric resistivity modeling and explain the mixed finite-element method. Next, we will explain the steepest descent method for our electric resistivity inversion technique on the basis of a matrix formalism (adjoint state) of the Poisson equation that is obtained in the process of solving for both electric potential and apparent electric field by the mixed finite-element method. Finally, we will generate subsurface images using our inversion algorithm for several block-anomaly models with a dipole–dipole array.

2. The governing equation and mixed finite-element method

2.1. Mathematical modeling

In an isotropic and conductive media, the equations describing the response due to a point current source $I_s(x,z)$ are expressed as

$$\nabla V(x,z) = -\rho(x,z)\mathbf{E}(x,z), \tag{1a}$$

$$\nabla \cdot \mathbf{E}(x,z) = I_s(x,z), \tag{1b}$$

where $V(x,z)$ is the electric potential, $\mathbf{E}(x,z)$ is the electric field vector, and $\rho(x,z)$ is the resistivity function which is strictly defined as positive value:

$$0 < m \leqslant \rho(x,z),$$

where m is the positive constant. Let us restrict the whole space to a conductive half space Ω, where Ω is the bounded and open subset of $\mathscr{R}^2$ having a piecewise continuous boundary Γ ($=\partial\Omega$). Γ_1 denotes the

ground surface ($z = 0$) and $\Gamma_2 = \partial\Omega/\Gamma_1$ (Fig. 1). The governing first-order system for the electric resistivity problem in the domain Ω can be expressed by the following Poisson's equation with mixed boundary conditions [6].

$$\nabla V(x,z) = -\rho(x,z)\mathbf{E}(x,z) \quad \text{in } \Omega, \tag{2a}$$

$$\nabla \cdot \mathbf{E}(x,z) = \frac{I}{\Delta S}\delta(x - x_s)\delta(z - z_s) \quad \text{in } \Omega, \tag{2b}$$

$$\mathbf{n} \cdot \mathbf{E}(x,z) = 0 \quad \text{on } \Gamma_1, \tag{2c}$$

$$V(x,z) = 0 \quad \text{on } \Gamma_2, \tag{2d}$$

where I is the current in amperes, (x_s, z_s) is the coordinate of point source, ΔS is the elemental area about the charge-injected point, and $\mathbf{n}$ is the outer normal vector at the boundary of Ω. The boundary condition at the ground surface Γ_1 is equivalent to the Neumann boundary condition for the electric potential

$$\left.\frac{\partial V}{\partial \mathbf{n}}\right|_{\Gamma_1} = 0. \tag{3}$$

Though the Dirichlet boundary condition used in Eq. (2d) is only valid at infinity, Eq. (2d) can be used if the domain is far away from the sources [19]. The Robin boundary condition as well as the Dirichlet and Neumann boundary conditions can also be used [6].

2.2. Mixed finite-element method

As shown in Fig. 2, we divide the region by the triangular element. The mixed finite-element equation with P_1–P_0 pair for triangular elements [3] for dc problem is

$$\mathbf{K}\mathbf{u} = \mathbf{r}, \tag{4}$$

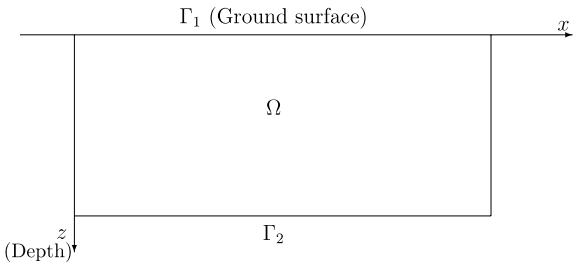

Fig. 1. Domain where electric resistivity exploration is experimented. Ω is a computational domain, Γ_1 is the ground surface boundary and Γ_2 is an artificial boundary.

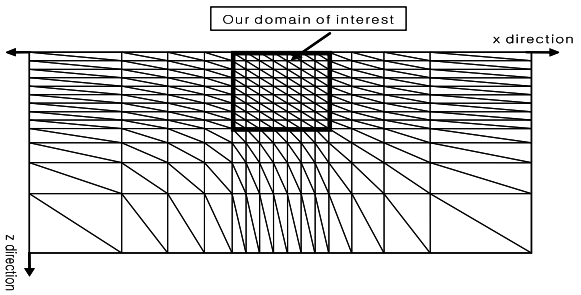

Fig. 2. Two-dimensional mesh and triangular elements in Ω.

with

$$\mathbf{K} = \begin{bmatrix} \mathbf{A} & \mathbf{B} \\ \mathbf{B}^{\mathrm{T}} & 0 \end{bmatrix},$$

where $\mathbf{A}$ is the mass matrix, $\mathbf{B}$ is the stiff matrix, $\mathbf{u}$ is the finite-element approximate solutions for the electric potential and electric field vector, and $\mathbf{r} = [\mathbf{0}\ \mathbf{s}]^{\mathrm{T}}$ is the source vector, which the vector $\mathbf{s}$ is induced by the source function in Eq. (2). And

$$\mathbf{A} = \int_{\Omega} \rho(x,z)\mathbf{N}^{\mathrm{T}}\mathbf{N}\,\mathrm{d}s,$$
$$\mathbf{B} = \int_{\Omega} \mathbf{N}^{\mathrm{T}}\mathbf{M}\,\mathrm{d}s,$$

where $\mathbf{N}$ is a row vector of shape function for electric field vector and $\mathbf{M}$ is the gradient vector for electric potential. We know that $\mathbf{K}$ is the symmetric capacity matrix because $\mathbf{A}$, $\mathbf{B}$ are symmetric. Let $\mathbf{u} = [\mathbf{e}\ \mathbf{v}]^{\mathrm{T}}$ which the vectors $\mathbf{e}$ and $\mathbf{v}$ are the approximate solutions of electric field vector and electric potential, respectively. Then we obtain the electric field vector $\mathbf{e}$ and the electric potential $\mathbf{v}$ from Eq. (5)

$$\mathbf{B}^{\mathrm{T}}\mathbf{A}^{-1}\mathbf{B}\mathbf{v} = -\mathbf{s}, \tag{5a}$$
$$\mathbf{e} = -\mathbf{A}^{-1}\mathbf{B}\mathbf{v}. \tag{5b}$$

Since we choose the constant shape function for electric field vector, we note that $\mathbf{A}$ is a diagonal matrix. The computing time required for obtaining electric field vector and electric potential is compatible with that required when we use other numerical methods (finite-element or finite-difference method). Eq. (4) can be solved by LU decomposition for two-dimensional problems, but for three-dimensional problems, we can use the iterative incomplete Cholesky conjugate method [25,34] to minimize the computer memory requirement and computation time.

3. Apparent electric field

3.1. Dipole–dipole array

In the dipole–dipole array frequently used in resistivity surveys as shown in Fig. 3, direct current I is passed into the subsurface at a dipole (C_1, C_2), while we measure the electric potential difference ΔV at the other dipole (P_1, P_2). The apparent resistivity ρ_{a} is defined in terms of both the current I and voltage ΔV as

$$\rho_{\mathrm{a}} = G\frac{\Delta V}{I}, \tag{6}$$

where $1/G$ is the geometric factor and G is expressed in the three-dimensional space as

$$G = \pi n(n+1)(n+2)a, \tag{7}$$

where n is the electrode separation index.

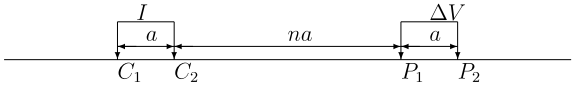

Fig. 3. Dipole–dipole array in two-dimensional dc resistivity exploration. Direct current I is passed into the subsurface at a dipole (C_1, C_2), while we measure the electric potential difference ΔV at the other dipole (P_1, P_2). Here n is the electrode separation index and a is the distance between dipole.

3.2. Apparent electric field at the flat ground surface

In a general resistivity inversion using the steepest descent method, we generally construct an objective function based on apparent resistivity and determine the steepest descent direction by computing the Jacobian matrix (described as partial derivatives of apparent resistivity with respect to a model parameter (resistivity)). On the other hand, in the case of using the backpropagation algorithm of the seismic inverse problem, the steepest descent direction is computed implicitly by using the adjoint state of the forward modeling operator [23]. In designing the resistivity inversion algorithm using the backpropagation technique, we first try to solve the inverse problem by backpropagating the electric potential difference of the Poisson equation, but we cannot use the adjoint state of the matrix formalism with the electric potential difference, since it is impossible to construct the partial derivative of the apparent resistivity from the capacity matrix derived from the standard finite-element method (Appendix A). For this reason, we adopt a new concept of an apparent electric field rather than apparent resistivity.

On the basis of the fact that the vertical electric field $E_z = 0$ at the flat ground surface (from the boundary condition in Eq. (2)) and that the horizontal electric field E_x can be approximated by $\Delta V/\Delta x$ if Δx is sufficiently small, we define the *apparent electric field* E_a as

$$E_a = E_x G_x, \tag{8}$$

where G_x acts as weighting function (having a similar effect as the automatic gain control in seismic data processing) at the ground surface. Selecting the appropriate weighting function (G_x) in Eq. (8) is subjective manner. For convenience, we modify the geometric factor into that which is conventionally used in a three-dimensional diploe–dipole survey. The modified weighting function G_x can be given as

$$G_x = \pi n(n+1)a.$$

Figs. 4(b) and (c) show apparent resistivities and horizontal components of apparent electric fields computed for the two-layer model as shown in Fig. 4(a). By comparing Fig. 4(c) with (b), we found that the horizontal components of apparent electric fields have similar features to apparent resistivities.

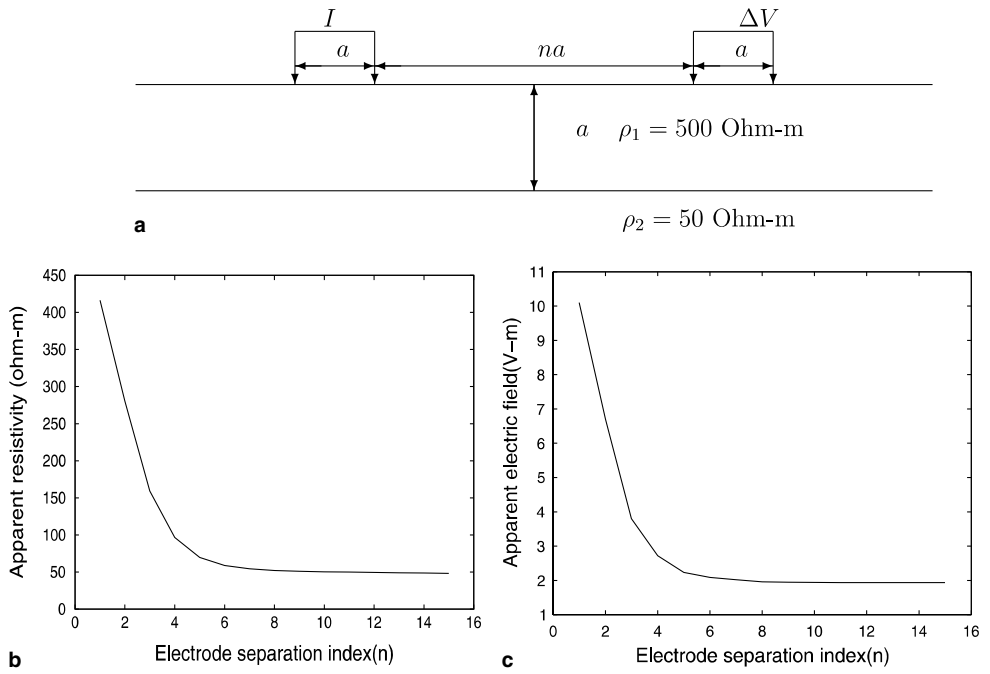

Fig. 4. (a) Dipole–dipole array in two-layer earth model whose size is 1 km × 0.2 km and electrode interval is 25 m, (b) apparent resistivity and (c) apparent electric field.

4. Inversion theory

4.1. Misfit function

In our resistivity inverse problem where the steepest descent method is used, we define the residual between the forward-modeled electric field vector and the finite-difference approximated electric field vector derived from measured voltage as follows:

$$\delta \mathbf{e}_x = \left(e_x^1 - \frac{\Delta v_{\text{obs}}^1}{\Delta x} \cdots e_x^n - \frac{\Delta v_{\text{obs}}^n}{\Delta x} \right)^{\mathrm{T}}, \tag{9}$$

where n is the number of receiver position, and for $j = 1, \ldots, n$, e_x^j is the horizontal component of the electric field vector computed for the current model, Δv_{obs}^j is the measured voltage, Δx is the intervals between electrodes grounded for measuring voltage. By parameterizing the subsurface by finite elements, we can identify the resistivity or conductivity at each element. In our algorithm, the model is characterized by the resistivity parameter vector $\boldsymbol{\rho} = (\rho_1, \ldots, \rho_M)^{\mathrm{T}}$, where M is the number of model parameters. As with general inverse problems, we define the objective function Ψ as the l_2-norm of residuals between the measured electric field vector and the modeled electric field vector:

$$\Psi(\boldsymbol{\rho}) = \frac{1}{2} \left(e_x^1 - \frac{\Delta v_{\text{obs}}^1}{\Delta x} \cdots e_x^n - \frac{\Delta v_{\text{obs}}^n}{\Delta x} \right) \begin{pmatrix} G_x^1 & 0 & 0 & 0 & 0 \\ 0 & G_x^2 & 0 & 0 & 0 \\ & & & & \\ 0 & 0 & \vdots & 0 & 0 \\ 0 & 0 & 0 & 0 & G_x^n \end{pmatrix} \begin{pmatrix} e_x^1 - \frac{\Delta v_{\text{obs}}^1}{\Delta x} \\ \vdots \\ e_x^n - \frac{\Delta v_{\text{obs}}^n}{\Delta x} \end{pmatrix}, \tag{10}$$

where G_x^j is given by Eq. (8) for $j = 1, \ldots, n$.

4.2. The steepest descent method

When using the steepest descent method, we iteratively update the model parameter using the following relationship as follows:

$$\rho_k^{l+1} = \rho_k^l - \alpha^l \frac{\partial \Psi^l}{\partial \rho_k}, \quad k = 1, \ldots, M, \tag{11}$$

where l is the iteration number and α^l is the step length arbitrary chosen and $\partial \Psi^l / \partial \rho_k$ is the direction perpendicular to the contours of the constant objective function.

The gradient $\partial \Psi^l / \partial \rho_k$ in Eq. (11) can be computed directly by calculating the partial derivative of apparent electric field with respect to resistivity. Following Rodi [24], Oristaglio and Worthington [18], and Pratt et al. [23], we can express the partial derivatives of the apparent electric field vector and electric potential as

$$\begin{aligned} &\frac{\partial \mathbf{K}}{\partial \rho_k} \mathbf{u} + \mathbf{K} \frac{\partial \mathbf{u}}{\partial \rho_k} = 0, \\ &\frac{\partial \mathbf{u}}{\partial \rho_k} = -\mathbf{K}^{-1} \frac{\partial \mathbf{K}}{\partial \rho_k} \mathbf{u}. \end{aligned} \tag{12}$$

In Eq. (12), we can define the kth virtual source as

$$\mathbf{f}^{(k)} = -\frac{\partial \mathbf{K}}{\partial \rho_k} \mathbf{u}. \tag{13}$$

Fig. 5 shows the partial derivatives where the virtual source is located at the center of the model and the source lies at the center of the ground surface. The steepest descent direction of our objective function can be expressed as

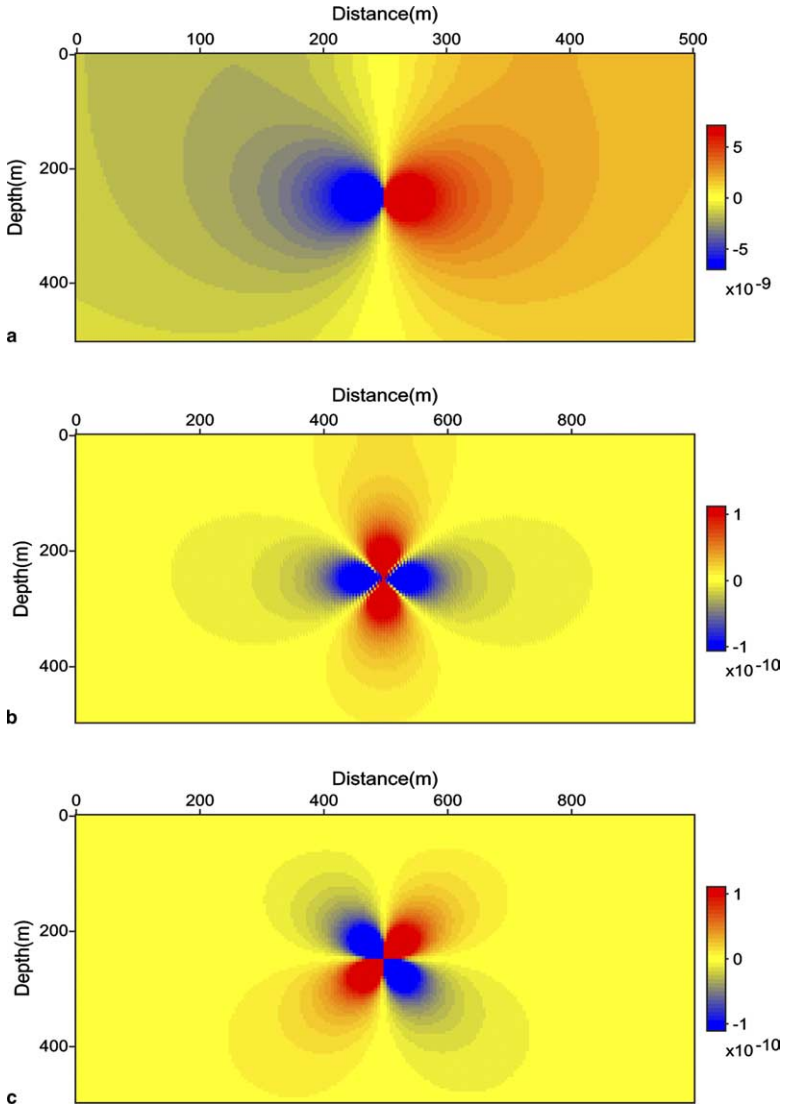

Fig. 5. (a) The Fréchet derivative $\partial V/\partial\rho_i$ of electric potential, (b) the Fréchet derivative $\partial E_x/\partial\rho_i$ of horizontal component of vector field, (c) the Fréchet derivative $\partial E_z/\partial\rho_i$ of vertical component of vector field, where we perturb the conductivity at the center of the model.

$$\frac{\partial\Psi}{\partial\rho_k} = \left[\begin{pmatrix} G_x^1 & 0 & 0 & 0 & 0 \\ 0 & G_x^2 & 0 & 0 & 0 \\ & & \vdots & & \\ 0 & 0 & 0 & 0 & 0 \\ 0 & 0 & 0 & 0 & G_x^n \end{pmatrix} \begin{pmatrix} \frac{\partial e_x^1}{\partial\rho_k} \\ \vdots \\ \frac{\partial e_x^n}{\partial\rho_k} \end{pmatrix}\right]^{\mathrm{T}} \begin{pmatrix} e_x^1 - \frac{\Delta v_{\mathrm{obs}}^1}{\Delta x} \\ \vdots \\ e_x^n - \frac{\Delta v_{\mathrm{obs}}^n}{\Delta x} \end{pmatrix}$$

$$= \begin{pmatrix} \frac{\partial e_x^1}{\partial\rho_k} & \cdots & \frac{\partial e_x^n}{\partial\rho_k} \end{pmatrix} \begin{pmatrix} G_x^1 & 0 & \cdots & 0 \\ 0 & \cdot & 0 & 0 \\ 0 & 0 & \cdot & 0 \\ 0 & 0 & 0 & G_x^n \end{pmatrix} \begin{pmatrix} \delta e_x^1 \\ \vdots \\ \delta e_x^n \end{pmatrix}, \quad k = 1, \ldots, M, \tag{14}$$

where $\delta e_x^j = e_x^j - \Delta v_{\mathrm{obs}}^j/\Delta x,\ j = 1, \ldots, n$. By augmenting zeroes to Eq. (14), we can express $\partial\Psi/\partial\rho_k$ as

$$\frac{\partial \Psi}{\partial \rho_k} = \left(\frac{\partial e_x^1}{\partial \rho_k} \cdots \frac{\partial e_x^N}{\partial \rho_k} \frac{\partial e_z^1}{\partial \rho_k} \cdots \frac{\partial e_z^N}{\partial \rho_k} \frac{\partial v_x^1}{\partial \rho_k} \cdots \frac{\partial v_x^L}{\partial \rho_k} \right) \begin{pmatrix} G_x^1 & 0 & \cdots & 0 & \cdots & 0 & 0 & 0 \\ 0 & \cdot & 0 & 0 & 0 & 0 & 0 & 0 \\ 0 & 0 & \cdot & 0 & 0 & 0 & 0 & 0 \\ 0 & 0 & 0 & G_x^n & 0 & 0 & 0 & 0 \\ 0 & 0 & 0 & 0 & 0 & 0 & 0 & 0 \\ & & & & & \vdots & & \\ 0 & 0 & 0 & 0 & 0 & 0 & 0 & 0 \end{pmatrix} \begin{pmatrix} \delta e_x^1 \\ \vdots \\ \delta e_x^n \\ 0 \\ \vdots \\ 0 \\ 0 \\ \vdots \\ 0 \end{pmatrix}, \tag{15}$$

where N is the number of electric field vector, L is the number of electric potential. By following Pratt et al.'s notation [23], we again write Eq. (15) as

$$\frac{\partial \Psi}{\partial \rho_k} = \left(\widetilde{\mathbf{G}} \frac{\partial \mathbf{u}}{\partial \rho_k} \right)^{\mathrm{T}} \delta \widetilde{\mathbf{e}}, \tag{16}$$

which

$$\widetilde{\mathbf{G}} = \begin{pmatrix} G_x^1 & 0 & \cdots & 0 & \cdots & 0 & 0 & 0 \\ 0 & \ddots & 0 & 0 & 0 & 0 & 0 & 0 \\ 0 & 0 & \ddots & 0 & 0 & 0 & 0 & 0 \\ 0 & 0 & 0 & G_x^n & 0 & 0 & 0 & 0 \\ 0 & 0 & 0 & 0 & 0 & 0 & 0 & 0 \\ & & & & & \vdots & & \\ 0 & 0 & 0 & 0 & 0 & 0 & 0 & 0 \end{pmatrix}, \quad \frac{\partial \mathbf{u}}{\partial \rho_k} = \begin{pmatrix} \frac{\partial e_x^1}{\partial \rho_k} \\ \vdots \\ \frac{\partial e_x^N}{\partial \rho_k} \\ \frac{\partial e_z^1}{\partial \rho_k} \\ \vdots \\ \frac{\partial e_z^N}{\partial \rho_k} \\ \frac{\partial v_x^1}{\partial \rho_k} \\ \vdots \\ \frac{\partial v_x^L}{\partial \rho_k} \end{pmatrix}, \quad \delta \tilde{\mathbf{e}} = \begin{pmatrix} \delta e_x^1 \\ \cdots \\ \delta e_x^n \\ 0 \\ \cdots \\ 0 \\ 0 \\ \cdots \\ 0 \end{pmatrix},$$

and $\widetilde{\mathbf{G}}$ is $(2N+L)\times(2N+L)$ diagonal matrix, $\partial \mathbf{u}/\partial \rho_k$ and $\delta \tilde{\mathbf{e}}$ are $(2N+L)\times 1$ vectors. Taking the transpose of Eq. (12) and substituting Eq. (12) into Eq. (16) give

$$\frac{\partial \Psi}{\partial \rho_k} = [\mathbf{K}^{-1}\mathbf{f}^{(k)}]^{\mathrm{T}} \widetilde{\mathbf{G}} \delta \widetilde{\mathbf{e}} = \mathbf{f}^{(k)^{\mathrm{T}}} [\mathbf{K}^{-1}]^{\mathrm{T}} \widetilde{\mathbf{G}} \delta \widetilde{\mathbf{e}} = \mathbf{f}^{(k)^{\mathrm{T}}} \left(\mathbf{K}^{-1} \widetilde{\mathbf{G}} \delta \widetilde{\mathbf{e}} \right), \quad k = 1, \ldots, M, \tag{17}$$

where $(\mathbf{K}^{-1})^{\mathrm{T}} = \mathbf{K}^{-1}$ (because $\mathbf{K}$ is symmetric). Since $\mathbf{K}$ is self-adjoint, the term $\mathbf{K}^{-1}\widetilde{\mathbf{G}}\delta\widetilde{\mathbf{e}}$ depicts the backpropagation of residuals of apparent electric fields. As a result, $\partial \Psi/\partial \rho_k$ can be obtained by the dot product between the virtual source $f^{(k)}$ and the backpropagated residual $\mathbf{K}^{-1}\widetilde{\mathbf{G}}\delta\widetilde{\mathbf{E}}$ in Eq. (17).

By substituting Eq. (17) into Eq. (11), we obtain the following equation:

$$\rho_k^{l+1} = \rho_k^l - \alpha^l \mathbf{f}^{(k)^{\mathrm{T}}} \left(\mathbf{K}^{-1} \widetilde{\mathbf{G}} \Delta \widetilde{\mathbf{e}} \right), \quad k = 1, \ldots, M. \tag{18}$$

In parameterizing the conductivity or logarithm of the resistivity or conductivity [30], the steepest descent direction will be in a similar form as Eq. (18) (Appendix B). If we use the Levenberg–Marquardt method [15] for introducing a damping term to regularize the steepest descent method, Eq. (18) should be rewritten as

$$\rho_k^{l+1} = \rho_k^l - \alpha^l [\mathrm{diag}(\mathbf{H}_{\mathrm{a}} + \lambda \mathbf{I})^{-1}]_k \mathbf{f}^{(k)^{\mathrm{T}}} (\mathbf{K}^{-1} \widetilde{\mathbf{G}} \Delta \widetilde{\mathbf{e}}), \quad k = 1, \ldots, M, \tag{19}$$

where $[\cdot]_k$ denotes the kth element of the diagonal components, $\mathbf{I}$ is the identity matrix, λ is the damping factor, and $\mathbf{H}_a$ is the Hessian, which can be approximated by $\mathbf{H}_a \approx \mathrm{diag}(\mathbf{J}^T\mathbf{J})$ [11,27]. In our algorithm, we replace the diagonal of the Hessian by a pseudo-Hessian proposed by Shin et al. [28].

4.3. Advantage of our proposed technique over the conventional Gauss–Newton method to DC problem

In calculating the steepest descent direction of the object function Ψ, Yi et al. [32], Tripp et al. [31] and Zhang et al. [36] calculated the Jacobian using the reciprocity of Green function. However, their approach required a great deal of saving, especially all of the Green functions, corresponding to source and receiver position, onto the hard disk or in computer memory. Suppose that n is the number of grid in the x, z or y (in three-dimensional case) directions. The total core memory needed to save Green's function for computation of partial derivative is $4mn^2$ byte memory for a two-dimensional problem, whereas $4mn^3$ byte memory for a three-dimensional problem, where m is the number of sources and receivers which are not overlapped. To the contrary, our technique needs only $8n^2$ byte memory in two-dimensional problem and $8n^3$ byte memory in three-dimensional problem, for saving both the backpropagating electric vector and forward-modeled vector. The operation counts for both techniques required to compute the steepest descent direction show almost the same (Appendix C). However, in case of the reciprocity approach we will encounter insurmountable overhead computing cost, in particular, for large scale three-dimensional problems because of memory or disk access latency in computing the partial derivative using the reciprocity theorem. Therefore, our approach has a great advantage over the reciprocity approach, in terms of computing cost, even though it provides the same operation counts for the computation of the steepest descent direction.

5. Numerical results

In order to examine our electric inversion algorithm for synthetic data, we take two simple two-dimensional models, which one is the model (model I) with a conductive body embedded in the homogeneous half space and the other is the model (model II) with two conductive bodies embedded in the homogeneous half space. The partial derivatives of apparent electric field with respect to the resistivity block $\boldsymbol{\rho}_\mathbf{B}$ can be obtained by

$$\frac{\partial \mathbf{E}_a}{\partial \boldsymbol{\rho}_\mathbf{B}} = \sum_{(i,j)\in\mathbf{B}} \frac{\partial \mathbf{E}_a}{\partial \rho(i,j)}.$$

For stop criterion, the RMS error $r(l)$ for iteration number l can be defined as

$$r(l) = \sqrt{\frac{\Psi^l(\boldsymbol{\rho})}{N}},$$

where N is the sum of the numbers of resistivity parameters and dipoles with sources and receivers. We stop the iteration when $r(l)/r(1)$ is less than 0.2 for cell parameterization and 0.1 for block parameterization. We experimented the inversion of synthetic data by both cell and block parameterization.

5.1. Model I: a rectangular block embedded in a homogeneous half space

The sizes of the surrounding homogeneous space and the conductive block are 720 m × 180 m and 200 m × 80 m, respectively (see Fig. 6(a)). The resistivities of the surrounding half space and the conductivity body are 500 and 50 Ωm, respectively. The electric resistivity inversions are experimented with 40 dipole–dipole array (electrode spacing 20 m). For the initial model, we use a homogeneous model of resistivity of 500 Ωm. Figs. 6(b) and (c) show the results inverted by the inversion algorithm using the backpropagation technique with a cell (whose size is 2 m × 2 m) and a block (whose size is 10 m × 10 m), respectively. Fig. 6 shows that when we use a small-size cell, we can obtain a smooth structure (because we have more unknowns than those of the block parameterization). From Fig. 6(c), we confirm that our inversion algorithm gives results compatible with the original structure even though we start from a homogeneous model.

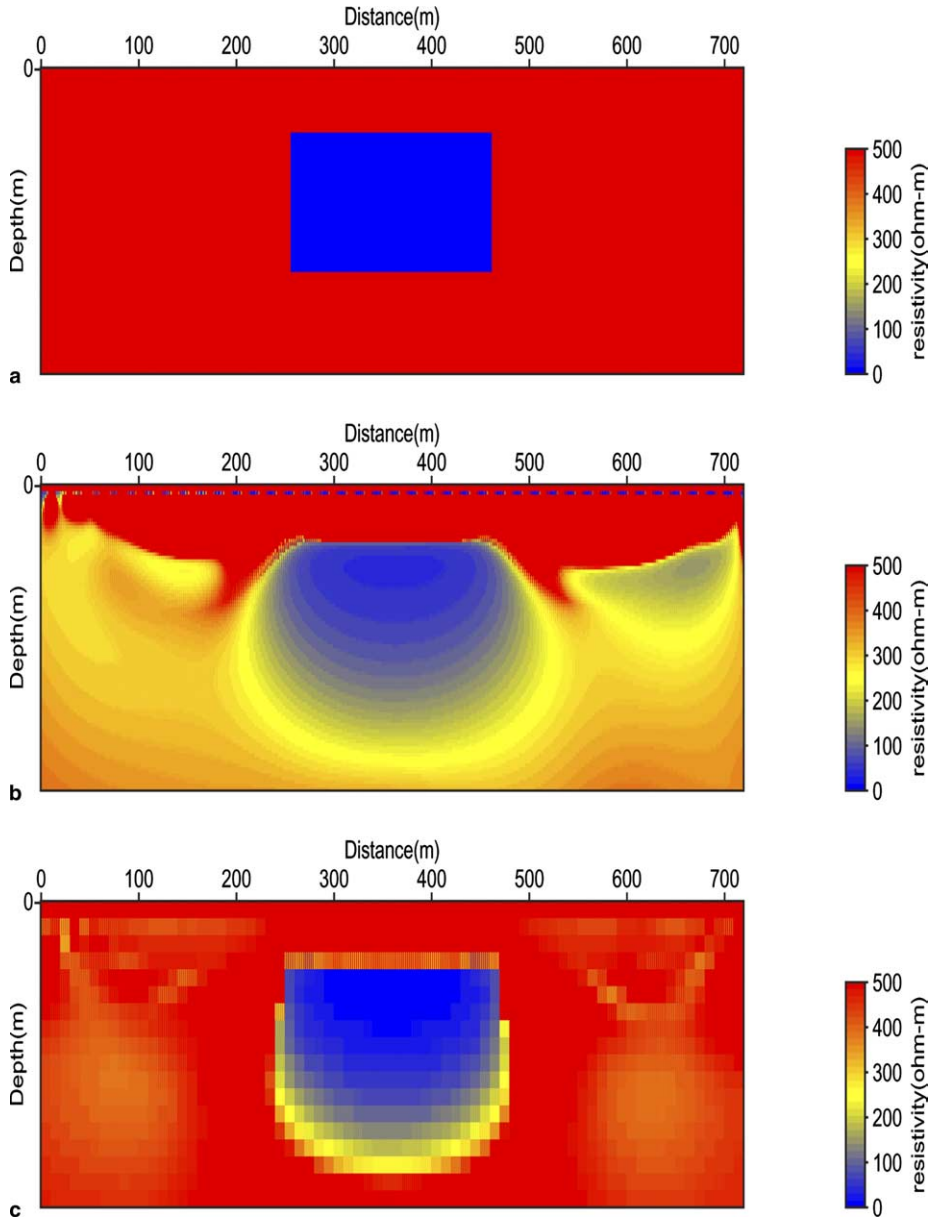

Fig. 6. (a) Two-dimensional true model used for resistivity inversion where the conductive block is located in 40 m depth from the earth surface, (b) the inverted result at 2274th iteration by the inversion algorithm by using backpropagation with the resistivity cell of 2 m × 2 m and (c) the inverted result at 1001th iteration with the resistivity block of 10 m × 10 m.

5.2. Model II: two rectangular blocks embedded in a homogeneous half space

The sizes of the surrounding homogeneous space and the two conductive blocks are 1000 m × 200 m and 176 m × 80 m, respectively (see Figs. 7–9(a)). The resistivity of the surrounding half space is 500 Ωm, whereas the resistivity of the left conductivity body is 50 Ωm and the resistivity of the right conductivity body is 150 Ωm. The electric resistivity inversions are experimented with 56 dipole–dipole array (electrode spacing 20 m), 27 dipole–dipole array (electrode spacing 40 m), 18 dipole–dipole array (electrode spacing 60 m), 13 dipole–dipole array (electrode spacing 80 m) and 11 dipole–dipole array (electrode

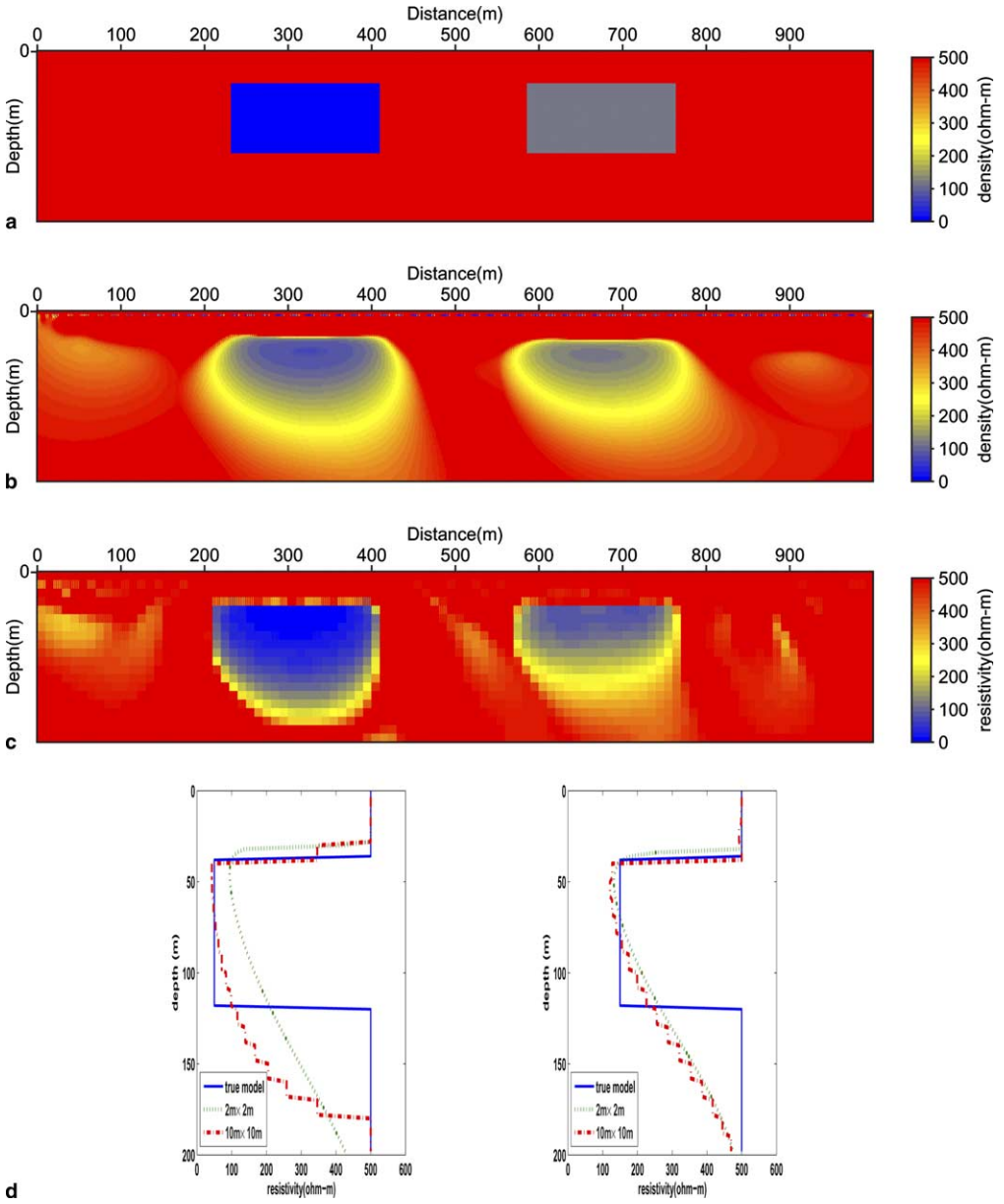

Fig. 7. (a) Two-dimensional true model used for resistivity inversion where both conductive blocks are located at a depth of 40 m from earth surface, (b) the inverted result at 1843th iteration by the inversion algorithm by using backpropagation with the resistivity cell of 2 m × 2 m, (c) the inverted result at 2004th with the resistivity block of 10 m × 10 m and (d) the resistivity according to a depth at 300 m point (left figure) and 660 m point (right figure).

spacing 100 m). For our inversion, we independently invert each experimental data and then averaging the inversion results obtained by each experiment. Our initial model is a homogeneous half space of resistivity 500 Ωm.

Figs. 7–9(a) show the true models used for our resistivity inversion. Figs. 7–9(b) display the results inverted by cell (whose size is 2 m × 2 m) parameterization of our algorithm, while Figs. 7–9(c) depict the inverted models by block (whose size is 10 m × 10 m) parameterization of our algorithm. Lastly, Figs. 7–9(d) show the resistivity profile as a function of depth at at 300 m point (left figure) and 660 m point (right figure). In these figures, the dashed line represents the resistivity profile of the true model, the

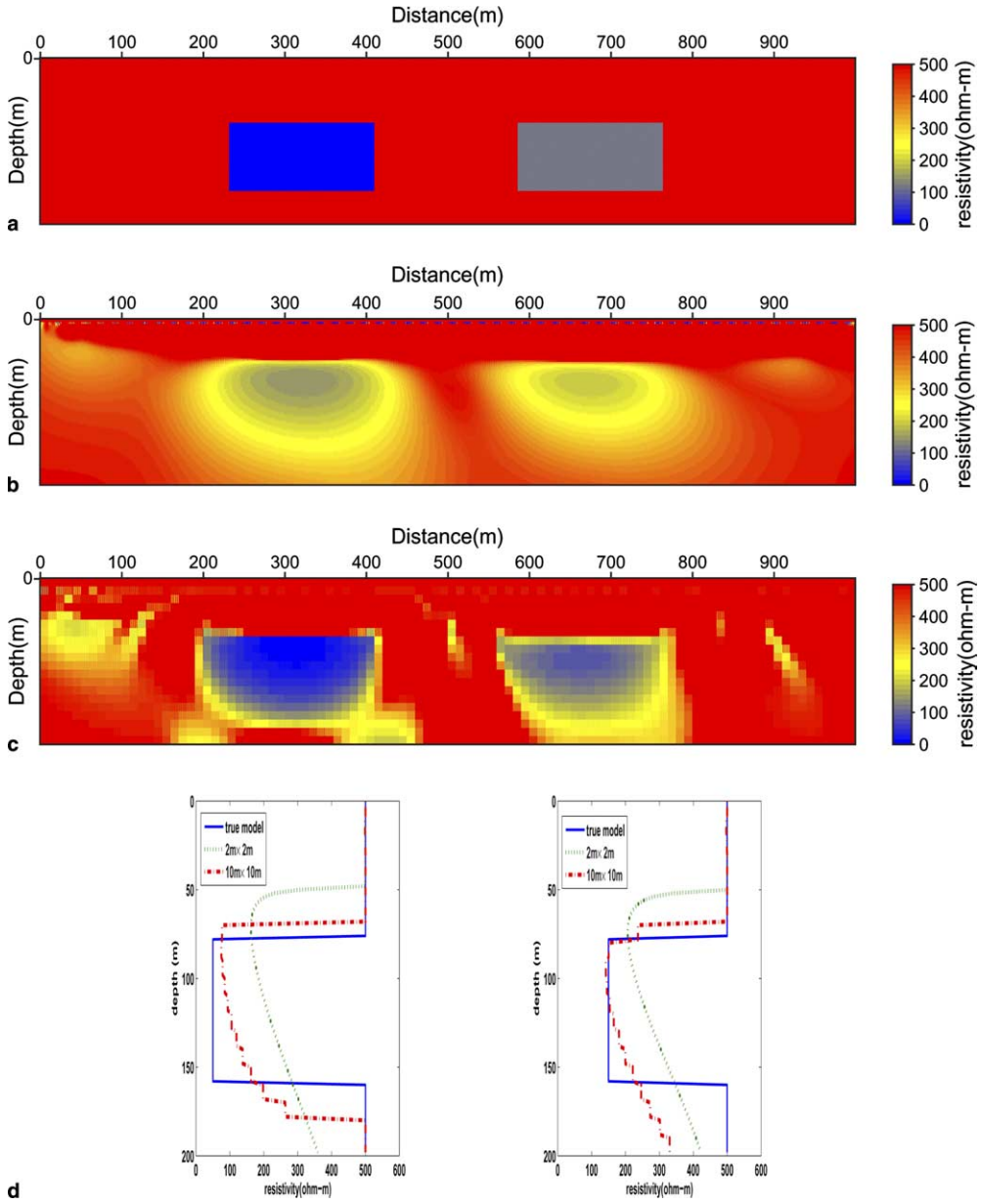

Fig. 8. (a) Two-dimensional true model used for resistivity inversion both conductive blocks are located at a depth of 80 m from earth surface, (b) the inverted result at 2270th iteration by the inversion algorithm by using backpropagation with the resistivity cell of 2 m × 2 m, (c) the inverted result at 2970th iteration with the resistivity block of 10 m × 10 m and (d) the resistivity according to depth at 300 m point (left figure) and 660 m point (right figure).

dotted corresponds to the resistivity profile by cell (2 m × 2 m) parameterization and the dotted dashed line corresponds to the resistivity profile by block (10 m × 10 m) parameterization. We know that with the inversion of small cell perturbation we can detect well enough the top of the conductivity bodies below the surface, but for the one far away from the surface we may not estimate the depth of bottom of the conductivity bodies. In case of block parameterization, we can have better delineation of the top and bottom of the conductivity bodies than the cell parameterization, regardless of the depth of the conductivity bodies.

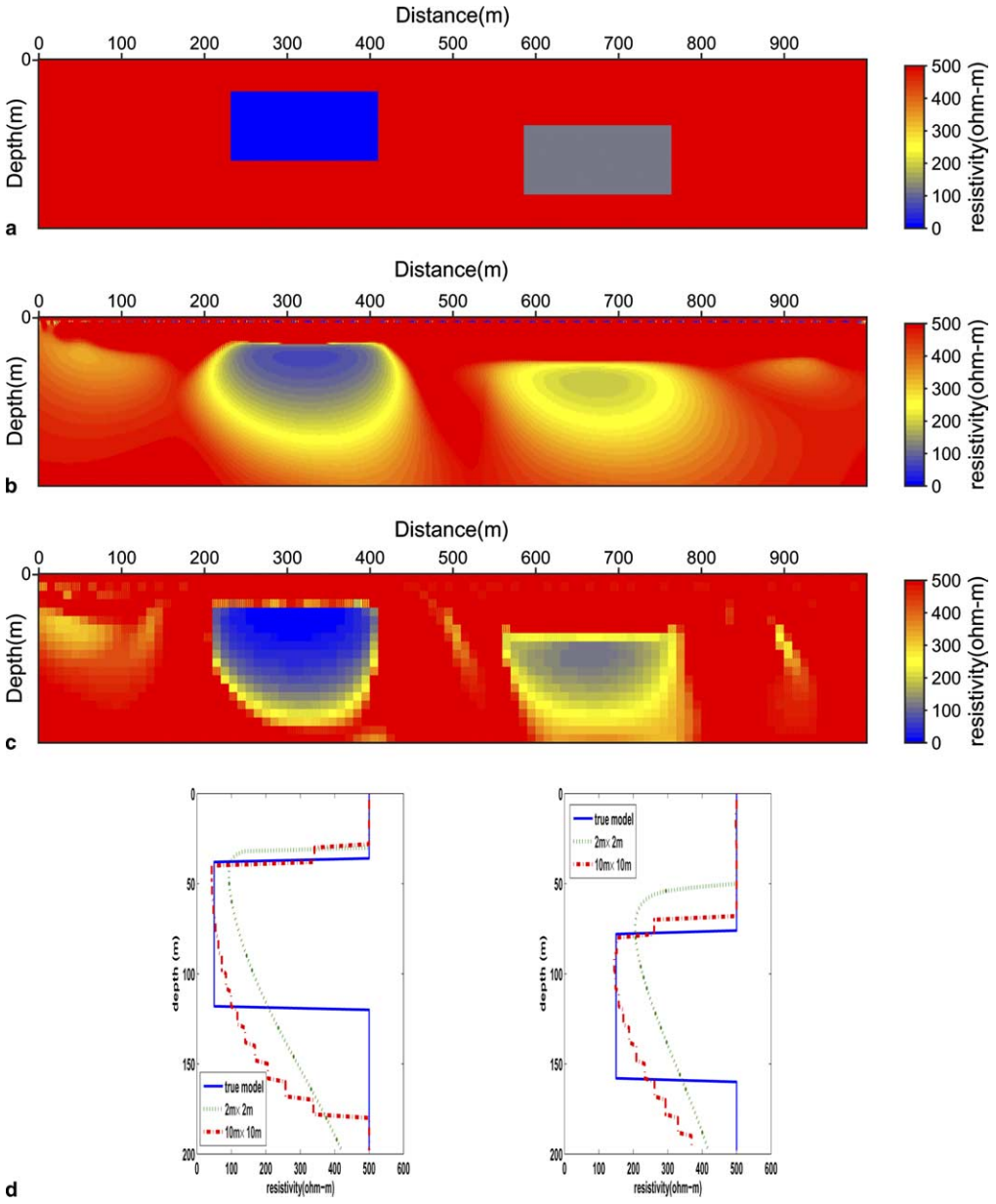

Fig. 9. (a) Two-dimensional true model used for resistivity inversion where one conductive block (left side) is located at a depth of 40 m from earth surface and the other (right side) is located at a depth of 80 m from earth surface, (b) the inverted result at 2518th iteration by the inversion algorithm using backpropagation with the resistivity cell of 2 m × 2 m, (c) the inverted result at 2371th iteration with the resistivity block of 10 m × 10 m and (d) the resistivity according to depth at 300 m point (left figure) and 660 m point (right figure).

6. Conclusions

We have proposed a new technique for inverting dc data in a similar way as it was done for the seismic waveform inverse problem using a backpropagation algorithm. In order to incorporate the backpropagation algorithm into the electric resistivity inverse problem, we used the electric field vector rather than apparent resistivity or electric potential difference, and had to use a mixed finite-element method with a $P_1 - P_0$ triangular element in order to maintain the adjoint state of the Poisson equation and to backpropagate the electric field vector and electric potential instead of electric potential difference.

Since exact electric field vector cannot be directly measured in field exploration, we define an apparent electric field as the dot product between the numerically computed electric field ($\Delta V/\Delta x$) and a weighting factor. The weighting factor plays a role of compensating attenuation caused by geometrical spreading. In our algorithm, the objective function is defined as the l_2-norm of residuals between the apparent electric fields computed for the initial model and the observed field data, while the steepest descent direction is computed by the product between virtual source and backpropagated residuals without computing the partial derivative directly. Therefore, our method has the advantage in that reduces its core memory to save Green's function and computing cost over the conventional Gauss–Newton method, even though the operation count of our method is nearly same to that of the method using the reciprocity theorem.

In our inversion algorithm, there is a wide choice of parameterization methods that vary from cell to block. From our numerical tests, we have noted that the inversion algorithm using backpropagation technique provides more lesser computation time and memory. In particular, we can obtain the good subsurface images through either the blocky cell parameterization or the small cell parameterization. The inversion with irregular topography or with anisotropic media demands an extensive future study.

Acknowledgments

The work of Ha was supported by the Korea Research Foundation Grant (KRF-2004-C00007) and the works of other people were financially supported by the National Research Laboratory Project of the Korea Ministry of Science and Technology, the Brain Korea 21 Project of the Korea Ministry of Education.

Appendix A. Why is it impossible to construct the partial derivative of the apparent resistivity from the standard finite-element method?

Let model parameter $\mathbf{p}$ be $(p_1,\ldots,p_M)$, the apparent resistivity measured at n receiver points $\boldsymbol{\rho}_a^d$ and the apparent resistivity calculated by the initial model $\boldsymbol{\rho}_a^m$. We define the misfit function Ψ by l_2-norm of errors of apparent resistivities:

$$\Psi(\mathbf{p}) = \tfrac{1}{2}(\boldsymbol{\rho}_a^d - \boldsymbol{\rho}_a^m)^T(\boldsymbol{\rho}_a^d - \boldsymbol{\rho}_a^m). \tag{A.1}$$

In the inversion algorithm using the steepest descent method, we try to find model parameter $\mathbf{p}$ to minimize Ψ. The gradient of the objective function with respect to model parameter p_i can be expressed as

$$\frac{\partial \Psi}{\partial p_i} = \left(\frac{\partial \boldsymbol{\rho}_a^m}{\partial p_i}\right)^T (\boldsymbol{\rho}_a^d - \boldsymbol{\rho}_a^m). \tag{A.2}$$

From Eq. (6), the partial derivative of $\boldsymbol{\rho}_a^m$ with respect to p_i is expressed as

$$\frac{\partial \boldsymbol{\rho}_a^m}{\partial p_i} = \frac{G}{I}\frac{\partial \Delta V}{\partial p_i}, \tag{A.3}$$

where $\frac{\partial \Delta V}{\partial p_i}$ can be obtained by numerical difference.

The capacity matrix arisen from the standard finite-element or finite-difference method can be given as [38]

$$\mathbf{S}\mathbf{v} = \mathbf{f}, \tag{A.4}$$

where $\mathbf{S}$ is the capacity matrix, $\mathbf{v}$ is the electric potential and $\mathbf{f}$ is a source. If we differentiate both sides of matrix equation (A.4) with respect to p_i, then we obtain

$$\frac{\partial \mathbf{S}}{\partial p_i}\mathbf{v} + \mathbf{S}\frac{\partial \mathbf{v}}{\partial p_i} = 0, \tag{A.5a}$$

$$\frac{\partial \mathbf{v}}{\partial p_i} = -\mathbf{S}^{-1}\frac{\partial \mathbf{S}}{\partial p_i}\mathbf{v}. \tag{A.5b}$$

From Eq. (A.5), we can see that $\frac{\partial \mathbf{v}}{\partial p_i}$ is not Fréchet derivative of electric potential difference (ΔV), as given in (A.3), but only Fréchet derivative of electric potential ($\mathbf{v}$). Because of this property of the standard finite-element or finite-difference method for Poisson's equation, we cannot implement the backpropagation technique of seismic

waveform inversion to the conventional finite-element or finite-difference method in an electric resistivity inversion scheme.

Appendix B. The steepest descent direction with respect to the conductivity or logarithm of the resistivity or conductivity

When we parameterize the conductivity, we replace ρ by $1/\sigma$. Therefore Eq. (1b) becomes to

$$\nabla V(x,z) = -\frac{1}{\sigma(x,z)}\mathbf{E}(x,z), \tag{B.1a}$$

$$\nabla \cdot \mathbf{E}(x,z) = I_s(x,z). \tag{B.1b}$$

By similar argument in Sections 2 and 4, we obtain the same form as Eq. (17). Here the capacity matrix $\mathbf{K}$ is calculated with Eq. (B.1).

In taking the logarithm of the resistivity or conductivity, we know that

$$\frac{\partial \mathbf{E}}{\partial \ln \rho} = \frac{1}{\rho}\frac{\partial \mathbf{E}}{\partial \rho} \quad \text{or} \quad \frac{\partial \mathbf{E}}{\partial \ln(1/\sigma)} = -\sigma\frac{\partial \mathbf{E}}{\partial \sigma}.$$

As a result, Eq. (18) becomes to

$$\ln \rho_k^{l+1} = \ln \rho_k^l - \alpha^l \frac{1}{\rho_k^l}[\mathbf{f}^{(k)^{\mathrm{T}}}(\mathbf{K}^{-1}\widetilde{\mathbf{G}}\Delta\widetilde{\mathbf{e}})], \tag{B.2a}$$

$$\ln \sigma_k^{l+1} = \ln \sigma_k^l + \alpha^l \sigma_k^l[\mathbf{f}^{(k)^{\mathrm{T}}}(\mathbf{K}^{-1}\widetilde{\mathbf{G}}\Delta\widetilde{\mathbf{e}})]. \tag{B.2b}$$

Appendix C. Operation counts

Let n be the number of grid in x or z directions in a computational domain. We consider the operation count of computing the steepest descent direction by applying the reciprocity theorem for only two-dimensional problem, since the extension to the three-dimensional problem is straightforward. With the assumption that we factor a sparse capacity matrix by a standard bandtype solver, the operation count of backward and forward solution phase for each sparse right-hand side vector is $2n^3$ [10]. Since both source and receiver are locally placed for the optimal acquisition of the field data, we only computed the Green function corresponding to the source and receiver positions. Then the total operation count for the computation of entire Green's function is $2mn^3$, where m is the number of source and receiver positions which are not overlapped.

The operation count for calculating the partial derivative using the reciprocity theorem is m^2n^2. The operation count for computing the steepest descent direction from the partial derivatives is m^2n^2. Therefore, the total operation count of the approach of the reciprocity theorem is $2(n+m)mn^2$. However, our technique showed to need $4mn^3$ operation for both forward modeling and backpropagation step. In practice, the difference in the operation counts between the reciprocity approach and our backpropagation technique is negligible (Table C.1).

Table C.1
Comparison of the operation count between reciprocity approach and our backpropagation technique, in the two dimensional problem

	Reciprocity technique		Backpropagation technique
Green's function	$2mn^3$	Forward modeling	$2mn^3$
Jacobian	m^2n^2	Backpropagation	$2mn^3$
Gradient	m^2n^2		
Total number	$2(n+m)mn^2$	Total number	$4mn^3$

References

[1] L. Alfano, Introduction to the interpretation of resistivity measurements for complicated structural conditions, Geophys. Prosp., Eur. Assn. Geosci. Eng. 7 (1959) 311–366.
[2] L. Borcea, Electrical impedance tomography, Inverse Problem 18 (2002) R99–R136.
[3] P.G. Ciarlet, J.L. Lions, Handbooks of Numerical Analysis, vol. II, 1991, Elsevier Science Publishers B.V. (Finite Element methods Part I).
[4] M. Cheney, D. Isaacson, J.C. Newell, Electrical impedance tomography, SIAM Rev. 41 (1) (1999) 85–101.
[5] J.H. Coggon, Electromagnetic and electrical modeling by the finite element method, Geophysics 36 (1971) 132–155.
[6] A. Dey, H.F. Morrison, Resistivity modeling for arbitrarily shaped two-dimensional structures, Geophys. Prosp. 27 (1979) 106–136.
[7] L.C. Enfield, D.S. Holder, Electrical impedance tomography of brain function: overview and technical considerations, Int. J. Bioelectromagn. 4 (2) (2002) 199–200.
[8] A.J. Fitzgerald, D.S. Holder, Leila Eadie, C. Hare, R.H. Bayford, A comparison of techniques to optimize measurement of voltage changes in electrical impedance tomography by minimizing phase shift errors, IEEE Trans. Med. Imaging 21 (6) (2002) 668–675.
[9] R.C. Fox, G.W. Hohmann, T.J. Killpack, L. Rijo, Topographic effects in resistivity and induced-polarization surveys, Geophysics 45 (1980) 75–93.
[10] G.H. Golub, C.F. Van Loan, Matrix Computations, third ed., Johns Hopkins University Press, 1996.
[11] T. Ha, C. Shin, Problems of constructing Hessian in waveform inversion, in: SEG International Exposition and Seventy Second Annual Meeting Conference and Technical Exhibition, 2002.
[12] P. Lailly, The seismic inverse problem as a sequence of before stack migrations, in: Conference on Inverse Scattering, Society for Industrial and Applied Mathematics, 1983, pp. 206–220.
[13] Y. Li, D.W. Oldenburg, Approximate 3-D inversion of E-scan dc resistivity data, Geophys. J. Int. 109 (1992) 343–362.
[14] Q. Ma, The boundary element method for 3-D dc resistivity modeling in layered earth, Geophysics 67 (2002) 610–617.
[15] D.W. Marquardt, An algorithm for least squares estimation of nonlinear parameters, J. Soc. Ind. Appl. Math. 11 (1963) 431–441.
[17] M. Okabe, Boundary element method for the arbitrary inhomogeneities problem in electrical prospecting, Geophys. Prosp., Eur. Assn. Geosci. Eng. 29 (1981) 39–59.
[18] M.L. Oristaglio, M.H. Worthington, Inversion of surface and borehole electromagnetic data for two-dimensional electrical conductivity models, Geophys. Prosp. 28 (1980) 633–657.
[19] C.C. Pain, J.V. Herwanger, M.H. Worthington, C.R.E. de Oliveira, Effective multidimensional resistivity inversion using finite element techniques, Geophys. J. Int. 151 (2002) 710–728.
[20] C.C. Pain, J.V. Herwanger, J.H. Saunders, M.H. Worthington, C.R.E. de Oliveira, Anisotropic resistivity inversion, Inverse Problem 19 (2003) 1081–1111.
[21] M. Pessel, D. Gibert, Multiscale electrical impedence tomography, J. Geophys. Res. 108 (B1) (2003) 2054.
[22] W.R. Petrick Jr., W.R. Sill, S.H. Ward, Three-dimensional resistivity inverse using alpha centers, Geophys. Prosp. 46 (1981) 1148–1162.
[23] R.G. Pratt, C.S. Shin, G.J. Hicks, Gauss–Newton and full Newton methods in frequency-space seismic waveform inversion, Geophys. J. Int. 133 (1998) 341–362.
[24] W.L. Rodi, A technique for improving the accuracy of finite element solutions for magnetotelluric data, Geophys. J. Roy. Astr. Soc. 44 (1976) 483–506.
[25] Y. Saad, Iterative Methods for Sparse Linear Systems, PWS Publishing Company, 1996.
[26] Y. Sasaki, 3-D resistivity inversion using the finite element method, Geophysics 59 (1994) 1839–1848.
[27] C. Shin, S. Jang, D.J. Min, Improved amplitude preservation for prestack depth migration by inverse scattering theory, Geophys. Prosp. 49 (2001) 592–606.
[28] C. Shin, K. Yoon, K.J. Marfurt, K. Park, D. Yang, H. Lim, S. Chung, S. Shin, Efficient calculation of a partial-derivative wavefield using reciprocity for seismic imaging and inversion, Geophysics 66 (2001) 1856–1863.
[29] A. Tarantola, Inversion of seismic reflection data in the acoustic approximation, Geophysics 49 (1984) 1259–1266.
[30] A. Tarantola, Inverse Problem Theory and Methods for Model Parameter Estimation, Society for Industrial and Applied Mathematics (SIAM) (2005).
[31] A.C. Tripp, G.W. Hohmann, C.M. Swift Jr., Two-dimensional resistivity inversion, Geophysics 49 (1984) 1708–1717.
[32] M. Yi, J. Kim, Y. Song, S. Cho, S. Chung, J. Suh, Three-dimensional imaging of subsurface structures using resistivity data, Geophys. Prosp. 49 (2001) 483–497.
[34] X. Wu, Y. Xiao, C. Qi, T. Wang, Computations of secondary potential for 3D DC resistivity modelling using an incomplete Choleski conjugate-gradient method, Geophys. Prosp. 51 (2003) 567–577.
[35] S.Z. Xu, S.K. Zhao, Y. Ni, A boundary element method for 2-D resistivity modeling with a point current source, Geophysics 63 (1998) 399–404.
[36] J. Zhang, R.L. Mackie, T.R. Madden, 3-D resistivity forward modeling and inversion using conjugate gradients, Geophysics 60 (1995) 1313–1325.
[37] S. Zhao, M.J. Yedlin, Some refinements on the finite-difference method for 3-D dc resistivity modeling, Geophysics 61 (1996) 1301–1307.
[38] O.C. Zienkiewicz, R.L. Taylor, The finite element method, fifth ed.The Basis, vol. 1, Butterworth-Heinemann, Oxford, 2000.